IMAGE-CHARGE EFFECTS ON BEAM HALO FORMATION AND BEAM LOSS IN A SMALL-APERTURE ALTERNATING-GRADIENT FOCUSING SYSTEM*

J. Zhou and C. Chen, MIT Plasma Science and Fusion Center, Cambridge, MA 02139, USA

Abstract

A new mechanism is identified for beam loss in an intense charged-particle beam in a small-aperture system. In particular, effects of image charges on chaotic particle motion and beam halo formation in small-aperture alternating-gradient focusing systems are studied analytically and computationally using a test-particle model. For a uniform density profile corresponding to a Kapchinskij-Vladimirskij distribution, nonlinear image-charge fields result in chaotic particle motion and the ejection of particles from the beam core into a halo. Detailed chaotic particle motion and structure of the particle phase space is studied, and the beam loss rate is computed for a long transport channel.

INTRODUCTION

An important aspect in the design of periodically focused beams in such accelerators is to prevent the beams from developing halos because they may cause beam losses to the conducting walls of the accelerating structures. The problem of halo formation and beam losses is of a serious concern in the design of small-aperture focusing transport systems that are often required in order to keep accelerator costs manageable. Two key mechanisms for halo formation have been studied using analytical models [1-3] and self-consistent simulations with particle-in-cell (PIC) techniques [4-7]. Until the present analysis, however, most published analytical results [1-3] on beam halo formation have been based on free-space models in which wall effects on halo formation have been ignored.

In this paper, we report a new mechanism for chaotic particle motion and halo formation in intense charge-particle beams. In particular, use is made of a test-particle model to investigate the dynamics of root-mean-squared (rms) matched intense charged particle beams propagating through an alternating-gradient quadrupole magnetic field and a small aperture. While the present model allows for nonuniform beams with elliptic symmetry, the effects of image charges on halo formation are illustrated with a uniform (KV) beam distribution [8]. It is shown that the image-charge-induced fields are nonlinear, and that they induce chaotic particle motion and halo formation.

TEST-PARTICLE MODEL

We consider an rms-matched continuous intense charged-particle beam propagating in the longitudinal direction through an alternating-gradient quadrupole magnetic field with axial periodicity length s in a perfectly conducting round pipe with radius R. The beam density is assumed to be $n = n\left(x^2/a^2 + y^2/b^2\right)$. An analytical expression for the scalar potential can be obtained for the assumed density profile [9],

$$\phi = -\pi abq \int_0^\infty \frac{ds}{\sqrt{(a^2+s)(b^2+s)}} \int_0^T n(T)dT \qquad (1)$$
$$+ \pi abq \left[\int_0^\infty \frac{ds}{\sqrt{(a^2+s)(b^2+s)}} \int_0^{T_1} n(T_1)dT_1 - 2ln\left(\frac{R}{r}\right)\int_0^\infty n(T_1)dT_1 \right]$$

where

$$T = x^2/(a^2+s) + y^2/(b^2+s), T_1 = x_1^2/(a^2+s) + y_1^2/(b^2+s),$$
$$r = (x^2+y^2)^{1/2}, x_1 = R^2 x/(x^2+y^2), \text{ and } y_1 = R^2 y/(x^2+y^2).$$

For the KV beam (Fig. 1), the periodic beam envelope functions $a(s) = a(s+S)$ and $b(s) = b(s+S)$ can be calculated from envelope equations [10]. Furthermore, in the paraxial approximation, the transverse equations of motion for an individual test particle can be obtained [3] with the potential in Eq. (1).

It is important to specify initial conditions for the test-particle motion that are consistent with the assumed beam density, which is accomplished by the particular choice of an initial distribution function [3] at $s = s_0$, i.e., $f_b(x,y,x',y',s_0) = N_b\delta(W-1)/\pi^2\varepsilon_x\varepsilon_y$, where $x' = dx/ds$, and W is the variable defined by $W = x^2/a^2 + (ax'-xa')^2/\varepsilon_x^2 + y^2/b^2 + (by'-yb')^2/\varepsilon_y^2$. Here, a, a', b, and b' denote the "initial" values at $s = s_0$.
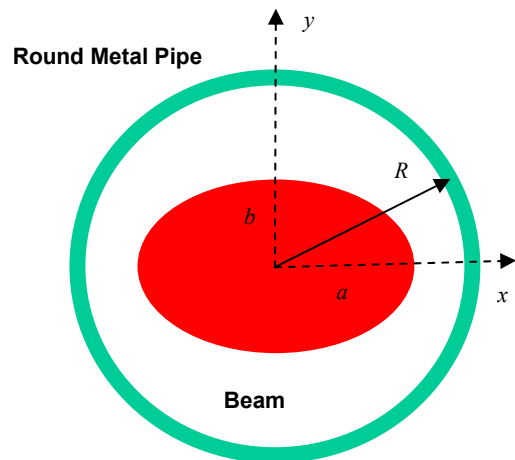

Fig.1 A uniform-densiyt beam with semi axes a and b corresponding to a KV distribution in a perfectly conducting round pipe of radius R.

IMAGE-CHARGE EFFECTS IN A LONG TRANSPORT CHANNEL

Using the model established in the previous section, we can investigate the halo formation and beam chaotic motion induced by the image-charge effects. For a long quadrupole focusing channel with the step-function lattice, the envelope functions $a(s)$ and $b(s)$ are obtained numerically and are benchmarked against the published results for the free-space case in [3]. The system parameters are chosen to be $\eta = 0.5$, $KS/\varepsilon_x = 10.0$, $\varepsilon_x = \varepsilon_y = \varepsilon$, and vacuum phase advance $\sigma_v = 80.0°$, which correspond to those in the High-Current Experiment (HCX) at LBNL [11].

The mechanism of beam loss is best illustrated by the phase space structure for the test-particle motion in the (x,x') plane as shown in Fig.2, where the Poincaré surface-of-section plots for the trajectories of test particles are demonstrated for two cases: (a) free-space ($\hat{R} \equiv R/\sqrt{\varepsilon S} = \infty$) and (b) $\hat{R} = 4.5$. Forty one and twenty nine test particles are loaded uniformly at $s = 0$ between the intervals $-2.0 \leq x' \leq 2.0$ and $-1.32 \leq x' \leq 1.32$ along the x'- axis in Figs. 2(a) and 2(b), respectively. Because all of the test particles have $(y(0), y'(0)) = 0$, their
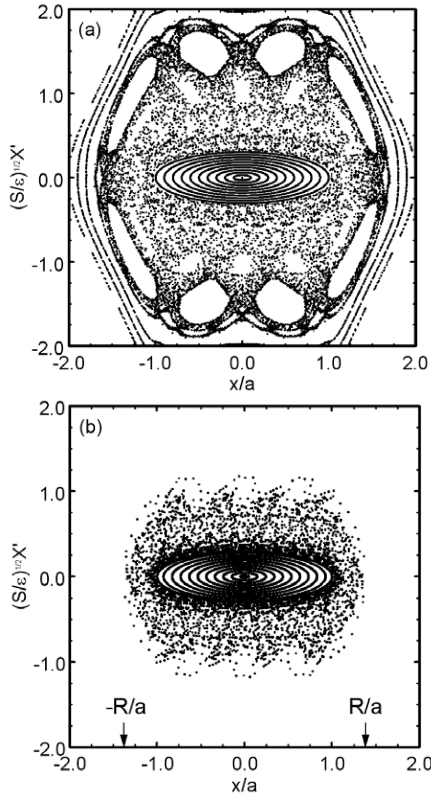

Fig.2 Poincaré surface-of section plots of test particles propagating over 1000 lattice periods in the phase plane (x, x') for two cases: (a) free-space $\hat{R} = \infty$ and (b) $\hat{R} = 4.5$.

trajectories remain in the (x,x') plane of the phase space. As shown in Fig.2 (a), well inside the beam with $W_x \leq 1$ the motion is regular, whereas there is a chaotic sea bounded between $W_x = 1$ and an outer Kolmogorov-Arnold-Moser (KAM) surface at $x/a = 1.7$ for the free-space case with $\hat{R} = \infty$. This chaotic sea is fully connected; that is, a particle in the chaotic sea will fill out the entire region if it travels for a sufficiently long distance. As the pipe radius R decreases, the conductor wall intersects the chaotic sea as shown in Fig.2 (b), in which case the particles in the chaotic sea will eventually strike the wall.

It should be pointed out that, as the pipe radius R decreases, the image effect on the dynamics of a beam with the KV distribution is subtle, as illustrated in Fig. 3. In Fig. 3 the transverse energy $W_x(s) = (x/a)^2 + (ax'/\varepsilon)^2$ is plotted as a function of the axial distance s for 50 test particles loaded at $s = 0$ on the beam boundary $W_x(0) = 1$ in the phase space with the initial phases $\phi_0 = \tan^{-1}[(S/\varepsilon)^{1/2} a(0)x'(0)/x(0)]$ uniformly distributed from 0 to $\pi/2$ for $\hat{R} = 4.5$. The system parameters are chosen to be the same as in Fig. 2. For the free-space case, the motion is stable, and the transverse energy is conserved with $W_x(s) = 1$ for all of the test particles. As R decreases to $\hat{R} = 4.5$, some test particles become chaotic due to the nonlinear force of the induced image charge on the wall, and the transverse energies of these particles are no longer constant.

The mechanism of image-charge-induced halo formation is further illustrated in Fig. 4 [10]. In Fig. 4, the range of W_x is plotted for test particles propagating over 2000 lattice periods for two cases: (a) free-space and (b) $\hat{R} = 3.8$. The system parameters are the same as in Figs. 2 and 3.
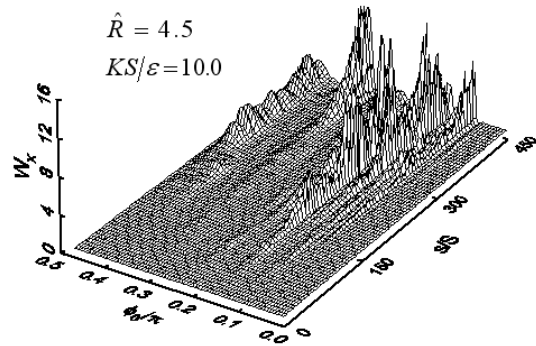

Fig. 3 Plots of W_x vs s for 50 test particles for $\hat{R} = 4.5$. The test particles are initially loaded uniformly with phase ϕ_0 ranging from 0 to $\pi/2$ on the beam boundary $(x(0)/a(0))^2 + (a(0)x'(0)/\varepsilon)^2 = 1$ in the phase space.
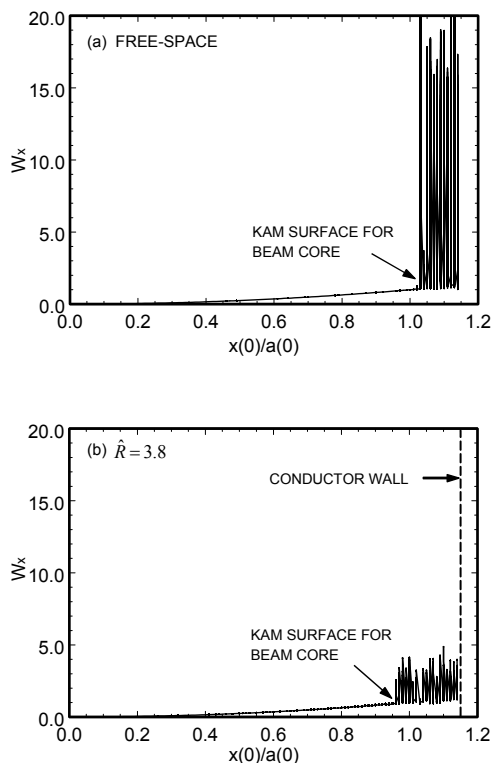
Fig. 4 Plots of the range of W_x for test particles propagating over 2000 lattice periods for two cases: (a) free-space and (b) $\hat{R} = 3.8$. The system parameters are the same as in Figs. 2 and 3. The 115 test particles are loaded uniformly at $s = 0$ between the interval $0 \le W_x \le 1.15$ along the x' axis in phase space.

Comparing the small-aperture case shown in Fig. 4(b) with the free-space case shown in Fig. 4(a), we find that, for both cases, the quantity W_x is constant for test particles well inside the beam interior with $0 \le x(0)/a(0) < 0.95$, and varies in a wide range for test particles outside the beam with $x(0)/a(0) > 1.03$. Near the beam edge with $0.95 < x(0)/a(0) < 1.03$, however, the quantity W_x shows different behavior. For the small-aperture case shown in Fig. 4(b), the fact that W_x is no longer a constant illustrates that this region of phase space is chaotic, and that the particle in the region will migrate outside the beam to form a halo.

The beam loss is computed as a function of propagation distance, and the results are shown in Fig. 5. The four curves correspond to four choices of the pipe radius with $\hat{R} = 3.8$, 3.9, 4.0, and 4.5. The beam loss rate increases. with the decreasing pipe radius, where the image effects play a more important role in the total space charge force. When the maximum beam envelope fills 86% of the pipe, the beam loss reaches 8% at $s = 1000S$.
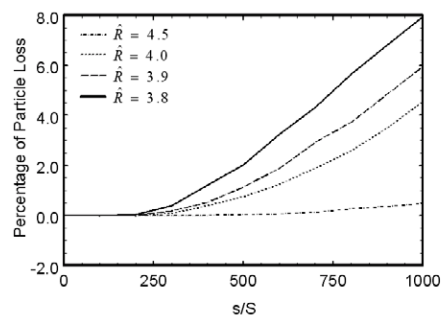

Fig. 5 Plots of the percentage of particles sticking the conductor wall as a function of propagation distance for several choices of $\hat{R} \equiv R/\sqrt{\varepsilon S}$. Here, 10,000 test particles with the KV distribution initially are used in the simulations.

CONCLUSION

We have shown using a test-particle model that in a small-aperture alternating-gradient focusing channel, image-charge effects induce a new mechanism for chaotic particle motion and halo formation in intense charge-particle beams. The percentage of beam loss has been calculated as a function of propagating distance and aperture size. Because our results are obtained for ideal KV distribution, they represent the minimum beam loss one may achieve in a long (>100 periods) focusing system such as the planned Integrated Research Experiment (IRE) for heavy ion fusion.

REFERENCES

1. R. L. Gluckstern, Phys. Rev. Lett. **73**, 1247 (1994).
2. J. M. Lagniel, Nucl. Instrum. Methods Phys. Res. **A345**, 405 (1994).
3. Q. Qian, R. C. Davidson, and C. Chen, Phys. Plasmas **2**, 2674 (1995); Phys. Rev. **E51**, R5216 (1995).
4. I. Haber, in *Proc. 1984 INS Int. Symposium on Heavy Ion Accelerators and Their Applications to Inertial Fusion* (Inst. Nuclear Study, Tokyo, 1984), p. 451.
5. C. M. Celata, in *Proc. 1987 Part. Accel. Conf.* (IEEE, New York, 1987), p. 996.
6. R. W. Garnett, *et al.*, *Space Charge Dominated Beams and Applications of High Brightness Beams*, edited by S. Y. Lee, AIP Conf. Proc. No. **377** (AIP, New York, 1996), p. 60.
7. T. P. Waggler and J. Qiang, *Advanced Accelerator Concepts*, edited by C. E. Clayton and P. Muggli (AIP, Mandalay Beach, CA 2002), p. 878.
8. I. Kapchinskij and V. Vladimirskij, in *Proceedings of the International Conference on High Energy Accelerators and Instrumentation* (CERN Scientific Information Service, Geneva, 1959), p.274.
9. J. Zhou, C. Chen, and B. L. Qian, Phys. Plasmas **10**, 4203 (2003).
10. B. L. Qian, J. Zhou, and C. Chen, Phys. Rev. ST Accel. Beams **6**, 014201 (2003).
11. P. A. Seidl, F. M. Bieniosek, C. M. Celata *et al.,* Nucl. Instrum. Methods Phys. Res. **A464**, 369 (2001).